Viral dispersal in the coastal zone: A method to quantify water quality risk

Peter E. Robins[a,*], Kata Farkas[b], David Cooper[c], Shelagh K. Malham[a], Davey L. Jones[b,d]

[a] School of Ocean Sciences, Bangor University, Marine Centre Wales, Menai Bridge LL59 5AB, UK
[b] School of Natural Sciences, Bangor University, Bangor LL57 2UW, UK
[c] Centre for Ecology and Hydrology, Environment Centre Wales, Bangor LL57 2UW, UK
[d] UWA School of Agriculture and Environment, University of Western Australia, Crawley, Australia

ABSTRACT

Waterborne and shellfish-borne enteric viruses associated with wastewater-polluted coastal waters (e.g. Norovirus, Hepatitis A/E viruses, Adenovirus) represent a major threat to human health. Improved understanding of the locations and periods of heightened risks can help target mitigation measures and improve public health. We developed a river-estuary-coast model to simulate virus dispersal, driven by point source discharges and river flows in combination with tidal forcing. Viral inputs were based on measured wastewater adenovirus concentrations and the model was implemented with or without viral die-off. We applied the model to the Conwy river (North Wales, UK), through the estuary, to the Irish Sea coast where bathing waters and shellfisheries are known to be prone to viral contamination. Using a suite of scenarios, we showed that river flow was the primary control of viral export to the coast. Since the Conwy catchment is short and steep, and the estuary is small and river-dominated, short-duration high intensity 'flash floods' were shown to transport viruses through the estuary and out to sea, despite dilution or die-off effects. Duplicating flow events (i.e., storm clustering) did not double the virus export since the virus re-entered the estuary on the flood tide. The tidal magnitude and timing of high water relative to peak river flow were also important drivers regulating viral dispersal. A worst-case event simulation (i.e., combining high river flows with high viral loading and high spring tide) resulted in increased concentrations of virus at nearby coasts, although the spatial spread was similar to the previous scenarios. Our results suggest that impact models for predicting and mitigating episodes of poor microbiological water quality may require careful representation of the intensity and timings of river flow when evaluating pathogen exposure risk.

1. Introduction

Current World Health Organisation figures estimate that globally 2.5 million deaths per year result from recreational contact with microbially contaminated water sources (Henry et al., 2016) and over 420,000 deaths are caused by foodborne disease – aquaculture in estuaries being a potential disease source (WHO, 2015). One of the main causes of waterborne and foodborne outbreaks of intestinal illnesses is enteric viruses which are transmitted via the faecal-oral route and are highly contagious. Infected individuals can shed the viruses at high concentrations and potentially pathogenic viruses are passed to wastewater treatment works. Commonly used secondary wastewater treatment processes (e.g. activated sludge and UV disinfection) are relatively inefficient at removing viruses (Kitajima et al., 2014; Qiu et al., 2015) and hence infectious viruses can enter the aquatic environment through wastewater discharge pipes and combined sewer overflows

(CSOs). Owing to urbanisation and increased wastewater discharge, enteric viruses are frequently detected in environmental waters including coastal and estuarine regions (Griffin et al., 2003; Hassard et al., 2016) posing a health risk to those engaged in recreational activities. Furthermore, shellfish destined for human consumption can ingest and bioaccumulate viruses which potentially lead to foodborne illnesses (Landry et al., 1983; Oliveira et al., 2011; Winterbourn et al., 2016). Increased pressure from pollution associated with urbanisation and population growth in some catchments, combined with projected impacts of climate change (e.g., Robins et al., 2016), has the capacity to change estuarine and coastal water quality processes, potentially increasing public health risk in the future.

Although the detection of all pathogenic viruses is possible through metaviromics, this approach is technically challenging, time-consuming and expensive (Adriaenssens et al., 2018). Consequently, indicator viruses are routinely used as proxies of general viral contamination of

* Corresponding author.
E-mail address: p.robins@bangor.ac.uk (P.E. Robins).

water bodies. Human norovirus has been proposed as one potential indicator of sewage contamination due to its proven link to shellfish-related food poisoning incidents, however, its seasonal wastewater discharge pattern makes it a poor year-round pollution indicator (Hassard et al., 2017). Human adenoviruses and polyomaviruses (usually causing asymptomatic infections) have also been used to track enteric viruses in the environment (Rachmadi et al., 2016; Rames et al., 2016). As these are enteric viruses, it is assumed that their transport and persistency are similar to other viruses causing severe symptoms. Current evidence indicates that adenoviruses are the enteric viruses most resistant to water treatment procedures (e.g., UV, chlorination) (Bofill-Mas et al., 2006; Linden et al., 2007; Eischeid et al., 2011) and most persistent in environmental waters (Charles et al., 2009; Rigotto et al., 2011), including estuarine and coastal waters where they remain persistent for several days or weeks (Enriquez et al., 1995; Wait and Sobsey, 2001). These findings suggest that adenoviruses are suitable as a worst-case example for modelling viral movements for environmental risk assessment.

Enteric viruses present in the river network may eventually reach estuaries after which their fate is largely unclear, being controlled by interactions of environmental conditions as well as their ability to decay over time. Understanding the conditions in which viruses may be retained in the estuary or transported offshore may significantly improve water quality management strategies and reduce public health risk. The subtle interactions of environmental conditions are by their nature site specific and no two estuaries will behave the same. For instance, small estuaries may be sensitive to flash flood events from rivers, whereby high virus loads are exported seaward in a matter of hours (e.g., Conwy, UK; Robins et al., 2014). On the other hand, larger estuaries (e.g., Humber, UK; Robins et al., 2018) will experience longer-duration river events because of the larger catchment size and will retain viruses in the estuary for longer subject to the strength of the estuarine circulation (Burchard et al., 2018; MacCready et al., 2018). Therefore, short bursts of heavy rainfall and prolonged periods of wet weather will impact virus transport through estuaries in markedly different ways depending on estuary type.

This means that modelling case studies with transferable methodologies are required to improve our understanding of viral movement and persistence. The aim of this study was to investigate the relative importance of some of the key processes influencing viral dispersal through a river-estuary-coast system by applying a hydrodynamic model to simulate fluxes at a national monitoring site (Conwy estuary, North Wales, UK). We consider both realistic and hypothetical scenarios within a sensitivity framework designed to isolate individual processes and assess their respective effects on virus dispersal.

2. Materials and methods

2.1. Study area

The Conwy estuary on the north coast of Wales (Fig. 1) is fed by the river Conwy whose catchment has an area of 380 km^2, draining much of the Snowdonia mountain range. The catchment is largely impermeable with large elevation gradients and high annual precipitation (up to 3500 mm), leading to rapid river flow responses to heavy rainfall (taking < 12 h for rainfall to reach the estuary; Robins et al., 2018). The river Conwy has a mean flow of 20 m^3 s^{-1}, with Q95 and Q10 (percentile flows) of 1.35 and 45.3 m^3 s^{-1}, respectively, as measured over the period 1965–2005 (Robins et al., 2014). A full description of the catchment geology, land use, population density, and chemical and biological water quality water is provided in Emmett et al. (2016).

The Conwy is a shallow and well-mixed, macro-tidal, embayment-type estuary, approximately 20 km in length. The estuary mouth has a large spring tidal range in excess of 6 m and a neap tidal range that is lower than 4 m. Under low river flow conditions, the tidal volume exchange dominates over the river input (Davidson et al., 1991). Strong

tidal mixing results in a vertically near-homogeneous salinity structure for the majority of the tidal cycle (Scott, 1994; Simpson et al., 2001; Howlett et al., 2015). During high flow events, the transport of riverborne material through the estuary is largely determined by river flow, with lesser tidal modification and with high sensitivity to sub-daily river flow variability (Robins et al., 2018). We retained bathymetric data for model development, and extensive observational data enabling model validation and input parameterisation (see Robins et al., 2014).

There are seven commercial mussel shellfish beds and four tourist beaches in the Conwy estuary mouth, located in a large expanse of shallow intertidal sand flats and deeper channels (Fig. 1, and also marked as S1–S7 and B1–B4 on Fig. 4). There are two major upstream wastewater treatment works (WWTWs) and approximately 35 CSOs along the river and the estuary which are known to be possible sources of viral accumulation in mussels. The frequency with which each CSO is activated varies between a few times per year to several times per month during normal weather conditions.

2.2. Virus input to the estuary from the catchment

Samples of wastewater, surface water, sediment and shellfish were collected monthly from March 2016 to August 2017 and analysed for human enteric viruses, including adenovirus (see Fig. 1 for our sampling sites). Further survey details and findings are summarised in Farkas et al. (2018). Firstly, we measured adenovirus at four sources which correspond to the sampling points shown in Fig. 1: (S1) Llanrwst WWTW; (S2) Betws-y-Coed WWTW; (S3) the river Llugwy upstream of Betws-y-Coed; and (S4) the river Conwy upstream of its confluence with the Llugwy. Next, we obtained flow measurements every 15 min from four locations (Fig. 1): (F1) sewage outflow from the Llanrwst WWTW; (F2) sewage outflow from the Betws-y-Coed WWTW; (F3) the river Conwy at Cwm Llanerch; and (F4) the river Lledr at Gethin's Bridge (provided by the government agency, Natural Resources Wales). Flow measurements at the two WWTWs (F1 and F2) coincided with the two adenovirus sampling points (S1 and S2). Finally, we estimated the flow at S3 and S4. We estimated flow in the Llugwy (S3) as equal to the flow in the river Lledr (F4). The Llugwy and Lledr are similar in catchment area and rainfall, and evidence from modelling suggests their flow regime is similar. The flow at S4 was estimated by the difference between the flow in the Conwy at Cwm Llanerch (F3) and the estimated flow in the Llugwy (F4). This provided 15 min estimates of flow at the four major sources/inputs of virus to the river network (S1–S4).

The virus concentration data available in water samples were three seasonal sets of 2-hourly measurements over three days at each WWTW, together with individual monthly values at the two WWTWs and two river sampling sites (S1–S4; Fig. 1). Other sources of viruses between these WWTWs and the tidal limit are assumed to be very small (e.g. from septic tanks). The data from this sampling programme are not sufficient support testing the statistical properties of any 15-min sequence of simulations, other than very approximately, but can provide credible scenario values. This is supported by the study of Farkas et al. (2018) showing no significant diurnal changes in bihourly-sampled adenovirus concentration in the treated wastewater effluent from Llanrwst and Betws-y-Coed WWTWs. We therefore generate sequences with the approximate properties of the measured data, without being able to fully assess their statistical properties with respect to true values. We took two approaches to generating scenario 15 min sequences of source virus concentrations (expressed as particle per litre; ppl).

In the first approach, we simulate 15 min virus concentrations, expressed as logarithms, to be the sum of two lag 1 auto-correlated sequences. The first sequence is defined at a 15 min scale and is generated with lag 1 autocorrelation (α) 0.9 and an error sequence (ε) of independent normally distributed random variables with mean zero, standard error estimated from the sample standard error of the 2-hourly values. This series approximates the behaviour of the within-day
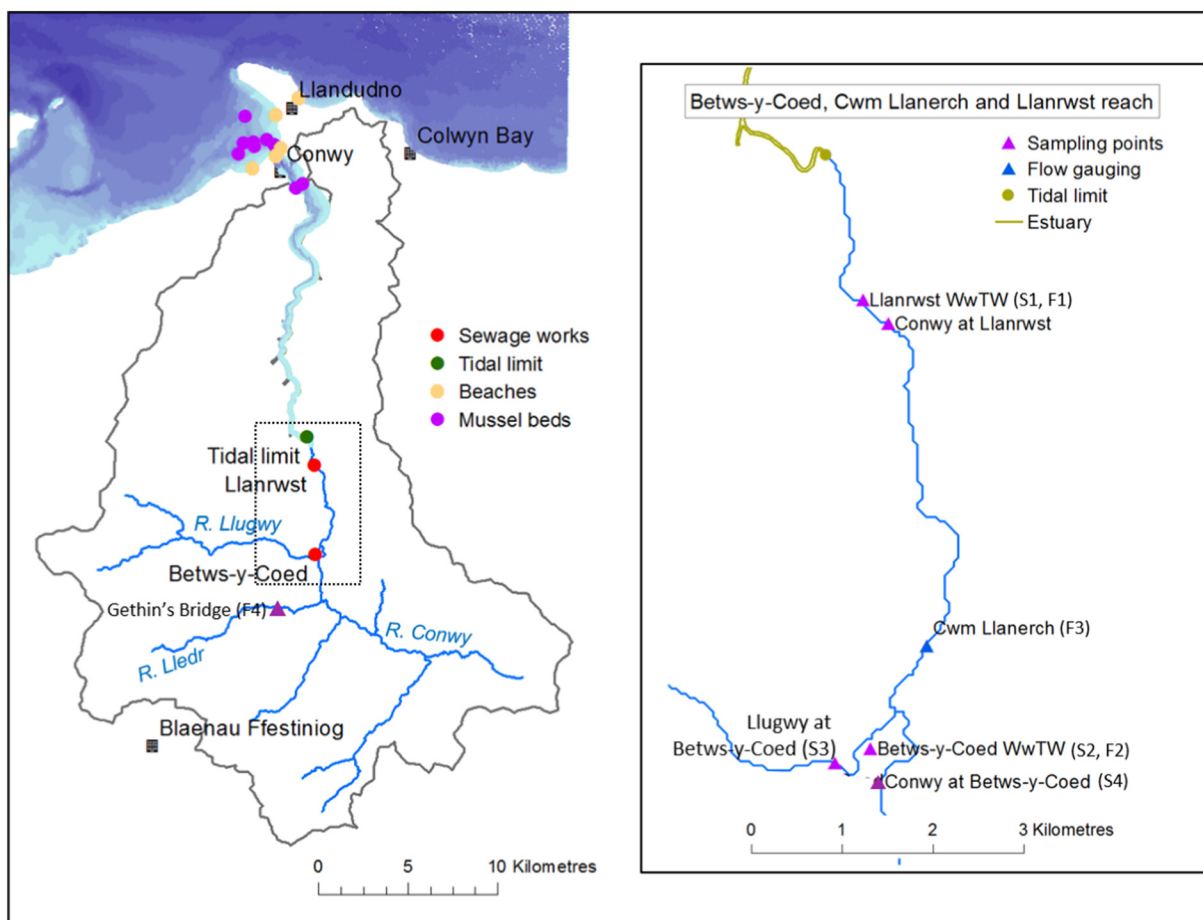
Fig. 1. Map of the Conwy estuary and catchment, and surrounding north Wales coast (UK). Shading offshore signifies water depth (light blue = shallow, dark blue = 30 m). Sewage works (WWTW), tourist beaches and commercial mussel beds are shown. The inset map (dashed lines) shows the water sampling and flow gauging stations. (For interpretation of the references to color in this figure legend, the reader is referred to the web version of this article.)

measurements about their mean value. The second sequence is daily, with lag 1 autocorrelation 0.5 and an error sequence of independent normally distributed random variables with mean and standard deviation estimated from the monthly measured data. This approximates the statistical behaviour for daily virus concentration that is consistent with the monthly measured values. In both cases, the model used here has the form:

$$y_t = \alpha y_{t-1} + \varepsilon_t$$
$$\varepsilon_t \sim N(0, \sigma^2)$$

For the daily sequence, y_t is adjusted for the logarithm of the estimated mean value, while for the 15 min sequence a zero mean is assumed. The two simulated auto-correlated sequences are summed and raised to the power 10 to generate the final simulations of virus concentrations at the WWTW outfalls. These are defined as Type 1 scenario estimates of virus concentrations.

While the Type 1 scenario sequences generated have the approximate statistical properties of the monthly and daily series, as calculated they are not constrained to fit the measured data. For further analysis, we condition the simulated daily sequence on the measured monthly values. The daily sequence generated then has the same statistical properties as calculated for Type 1 scenarios, but on those days when a measurement was made, the simulated and measured values correspond. To generate 15 min values we then interpolate the daily values using the loess routine of the R statistical package, rather than adding an auto-correlated 15 min sequence to the daily simulations. Conditioning was done piecewise for each period between monthly observations, with the constraint that the first and last simulated values

correspond to the measured value (on a logarithmic scale). These constrained simulations are defined as Type 2 scenario estimates virus concentrations.

Having generated 15 min scenario estimates of virus concentration for the four sources in the catchment, these were multiplied by the site flow estimates, and 15 min time series of flow and virus load were simulated at the tidal limit using the estimated travel time from each monitoring point. Statistical analysis was carried out using R statistical software (https://www.r-project.org/).

The load of viruses to the tidal limit of the Conwy was then taken to be the sum of contributions from four measured sources: In the first instance, it was assumed that the virus was conservative, remaining in the water column downstream of each monitoring location. Although high river flows can cause dilution of virus concentrations due to the increased freshwater fluxes, WWTWs may reach capacity and trigger CSOs which have the potential to release untreated sewage into the river network, in effect counteracting the dilution process. Due to insufficient observations, we have not included CSO influences in our study. The travel time of the viruses from each monitoring point to the tidal limit was estimated using the Manning equation, relating velocity to discharge through a power law relationship, which is a function of river slope and roughness. Slope was estimated from a 50 m digital elevation model (DEM), hydraulic radius from field observations of the river profile, and we used a Manning n value of 0.05 based on observed river characteristics. Note that the travel times in the river are short in relation to residence times in the estuary. The effect of viral decay was also considered, however, the decay rate of adenovirus in estuarine water is unknown. Hence, viral decay was estimated as $T_{90} = 1$ day,

based on the decay rate of poliovirus in estuarine water (Wait and Sobsey, 2001). We acknowledge that more work needs to be done on the viral degradation (varying turbidity, salinity and solar radiation) in environmental waters to better understand viral inactivation and decay.

2.3. Estuary model

We used a vertically-averaged hydrostatic ocean model (Telemac Modelling System V7.2; www.opentelemac.org) to model the Conwy estuary and surrounding coast. Telemac uses an unstructured-mesh, which is mapped on to observational bathymetry data, with varying resolution; being very high within the estuary (approximately 15 m) and coarser offshore (50–500 m). The bathymetric data was obtained from several sources: (1) Admiralty data at 200 m spatial resolution (EDINA, 2008); (2) LIDAR data in intertidal regions at 10 m resolution (available from the UK Environment Agency); (3) multibeam surveys of the Menai Strait at 10 m resolution conducted by Bangor University in 2013; and (4) single-beam echosouder surveys of the sub-tidal Conwy estuary channel which was conducted by Bangor University in 2003.

The Telemac model is well suited to vertically-mixed coastal applications since the unstructured mesh can be optimised to adequately resolve coastal features and the model incorporates wetting/drying capabilities of inter-tidal regions. The model is based on the depth-averaged shallow water Saint-Venant equations of momentum and continuity, derived from the Navier-Stokes equations (Hervouet, 2007). The classical k-ε turbulence model has been adapted into vertically averaged form to include additional dispersion terms (Rastogi and Rodi, 1978); a constant internal friction coefficient of 3×10^{-2} m was implemented in Nikuradse's law of bottom friction (Hervouet, 2007). Turbulent viscosity was set to a constant with the overall viscosity (molecular + turbulent) coefficient equal to 10^{-6}.

The model was initially spun-up during one month to create a steady-state salinity balance under minimum river flow conditions for the Conwy (Q99 flow of $1 \, \mathrm{m^3 \, s^{-1}}$). Tidal forcing comprised the 13 primary harmonic constituents (M_2, S_2, N_2, K_2, K_1, O_1, P_1, Q_1, M_4, MS_4, MN_4, M_f and M_m), derived from the Topex/Poseidon TPXO global tidal database on a structured grid of $0.25°$ resolution (Egbert et al., 1994). Both surface elevation change and the deduced horizontal velocities were used at the boundaries. The salinity distribution from these spin-up simulations were used as initial conditions for all subsequent simulations. For all simulations hereafter, key parameters (depth, velocity, salinity, virus concentration) were output every 15 min. Comprehensive validation procedures have previously been conducted for hydrodynamics and salinity intrusion (see Robins et al., 2014) which test the suitability of the model in depth-averaged mode for application to the Conwy.

2.4. Model simulations

2.4.1. Run 1: annual simulation of viral dispersal

Initially, we simulated adenovirus concentrations flowing from the river through the estuary to the coast, over one year starting 01 March 2016. River forcing comprised measured flows and Type 1 estimates of virus concentrations (both at 15 min intervals). Realistic tidal predictions (elevations and depth-averaged velocities) were applied at the offshore model boundary as explained in Section 2.3 and propagated inshore to the estuary. Surge and wave effects were not simulated. This annual simulation enabled the seasonal variability in viral dispersal to be characterised throughout the estuary and over shellfish beds and beaches. We simulated virus concentrations, C, that were both conservative and with a decay function ($T_{90} = 1$ day) (see Table 1, Run 1.1), following the formula:

$$C = C_0 e^{-kt} \tag{1}$$

where C_0 is the initial virus concentration and $k = -\ln(0.1)/T_{90}$ is the decay rate.

2.4.2. Run 2: virus dilution in space

High flows can cause dilution of virus concentrations. To investigate the likely downstream impact of this, we compared the highest flow period of our baseline simulation (Run 1.1, 01–30 July 2016) with a similar simulation but with virus dilution (Type 2 simulations). Again, we performed the simulation with and without virus decay (Eq. (1)).

2.4.3. Run 3: influence of hydrology on viral dispersal

In these simulations, we chose a series of hypothetical virus dispersal scenarios based on contrasting river flow (e.g. to capture high rainfall and storm events). These scenarios simulated a 15 d period (see Table 1) with 15 min river inputs. A mean tide was simulated, i.e., a principal lunar semi-diurnal (M_2) tide with an amplitude of 2 m. Unlike runs 1 and 2, we used a constant input virus concentration of 100 ppl but with virus decay (Eq. (1)). First, we investigated the influence of rainfall event clustering. We simulated a 'flash' river event (Run 3.1, see also Fig. 6b). This event was artificial but parameterised on the characteristics of the river Conwy – being of short duration (12 h) and with peak magnitude of $200 \, \mathrm{m^3 \, s^{-1}}$ (which is approximately the Q1 flow). River flows after the event were $1 \, \mathrm{m^3 \, s^{-1}}$ (Q99 flow). We compared this scenario with a 'storm cluster' scenario where the same flash event was repeated on consecutive days (Run 3.2; Fig. 6b). This comparison tested whether storm clustering has an additive effect on viral dispersal. We also compared the flash event (Run 3.1) with clusters of two smaller events (Run 3.3) and three smaller events (Run 3.4), see Fig. 6d. For these scenarios, the total freshwater volume flux was the same as for Run 3.1. To investigate the influence of rainfall intensity, we compared the flash event (Run 3.1) with a typically slow event with lower peak flow ($100 \, \mathrm{m^3 \, s^{-1}}$) but of longer duration (24 h) (Run 3.5), see Fig. 6f. Again, both these scenarios had an equal total freshwater volume flux. Typical flash and slow hydrograph shapes were derived by analysing a 35-year record for the Conwy river (see Robins et al. (2018) for further details).

2.4.4. Run 4: influence of the tide on viral dispersal

In this simulation, we varied the tidal forcing to test whether the semi-diurnal tidal cycle (i.e., flood vs. ebb) or lunar tidal cycle (i.e., spring vs. neap) influences viral dispersal. These simulations were forced with the principal semi-diurnal harmonic constituents M_2 and S_2 only. We compared four scenarios: (i) where spring high tide occurred during peak river flow (Run 4.1); (ii and iii) where spring high tide occurred 3 and 6 h after peak river flow (Run 4.2 and Run 4.3, respectively); and (iv) where neap high tide occurred during peak river flow (Run 4.4). For all cases, we used the flash river event, described as for Run 3.1 and constant input virus concentration of 100 ppl with virus decay (Eq. (1)).

2.4.5. Run 5: worst case scenario

Finally, we explored the impact of a combination event, where realistic river flows, tides and virus concentrations occurred in such a way as to produce a possible maximum virus export seawards (Run 5.1). We used Conwy river gauge measurements (15 min data from 1980 to 2010) to isolate the maximum freshwater inflow to the estuary (in terms of aggregated freshwater volume over 7 d). This occurred between 30 Jan–13 Feb 2004. We forced the simulation with TPXO global tidal data (see Section 2.3) for a period that contained the largest annual astronomical tides for 2016, which occurred on 11 April. Based on the results obtained from Runs 4.1–4.4 (see Section 3.4), we aligned the tide in such a way so that peak river flows coincided with peak ebb tidal flow. We used a constant virus concentration of 1×10^5 ppl (with virus decay; Eq. (1)), which was slightly higher than the maximum human adenovirus virus value ever measured in the river downstream of the Llanrwst WWTW.

Table 1
Summary of model simulations.

Run	Period	River flow	Tidal regime	Virus
1.1	Annual	01 Mar '16–01 Apr '17	01 Mar '16–01 Apr '17	Data-assimilated with/without decay
2.1	30 d	01–30 July 2016	01–30 July 2016	Data-assimilated with dilution and with/without decay
3.1	15 d	$1 \times$ flash hydrograph^{V1}	Mean tide (M2 only)	Constant ($= 100$ ppl) with decay
3.2		$2 \times$ flash hydrographs^{V2}		
3.3		$2 \times$ flash hydrographs^{V1}		
3.4		$3 \times$ flash hydrographs^{V1}		
3.5		$1 \times$ slow hydrograph^{V1}		
4.1	15 d	$1 \times$ flash hydrograph^{V1}	Spring-to-neap	Constant ($= 100$ ppl) with decay
4.2			Spring-to-neap ($+3$ h)	
4.3			Spring-to-neap ($+6$ h)	
4.4			Neap-to-spring	
5.1	15 d	30 Jan–13 Feb 2004^{V3}	11–26 Apr 2016	Constant ($= 1 \times 10^5$ ppl) with decay

[Freshwater volume 7 d-average entering estuary: V1 $= 3^7\,\text{m}^3$; V2 $= 6^7\,\text{m}^3$; V3 $= 9.7^7\,\text{m}^3$ – see also Fig. 6 hydrographs].

3. Results

3.1. Run 1: annual simulation of viral dispersal from river to coast

From our annual simulation, the most striking result was that the largest concentrations of viral export to the coast coincided with large river flow events (e.g., 01 Mar; 03 Apr; 09 Apr; 11 Jul; 22 Aug; 04 Sep; 11 Sep; 29 Sep; 20 Nov; 10 Dec) (Fig. 2). The largest virus export event occurred on 11 July 2016 with almost 1×10^3 ppl (particles per litre) dispersing offshore (Fig. 2e). This event corresponded with a period of particularly heavy rainfall, with three separate storms causing river flows to exceed $100\,\text{m}^3\,\text{s}^{-1}$ within one week of one another (Fig. 2b), amounting to a 7-day freshwater volume of $3.6 \times 10^7\,\text{m}^3$ (Fig. 2c). This event occurred between spring and neap tides (Fig. 2a). Hence, it would appear that the controlling factor on viral export was high river flows,

with the viral concentration input and the tidal state being of lesser importance.

The maximum river flow of $238\,\text{m}^3\,\text{s}^{-1}$ over the one year simulation period was measured on 22 August 2016 (Fig. 2b), although simulated virus export from the estuary was less than that during the 11 July event. Since simulated virus concentrations at source and tidal forcing were similar for both events, it is likely that the freshwater volume, the hydrograph shape, and the clustering of river events were important controls (e.g., the 22 Aug event followed two storms over a 7-day period and had 30% less freshwater volume than the 11 July event which followed three storms).

One of the largest estimated virus export events (20 Nov) occurred during neap tides and with less freshwater input than a smaller export event two weeks later (also during neaps). This variation could be caused by the different estimated concentrations of the virus from the
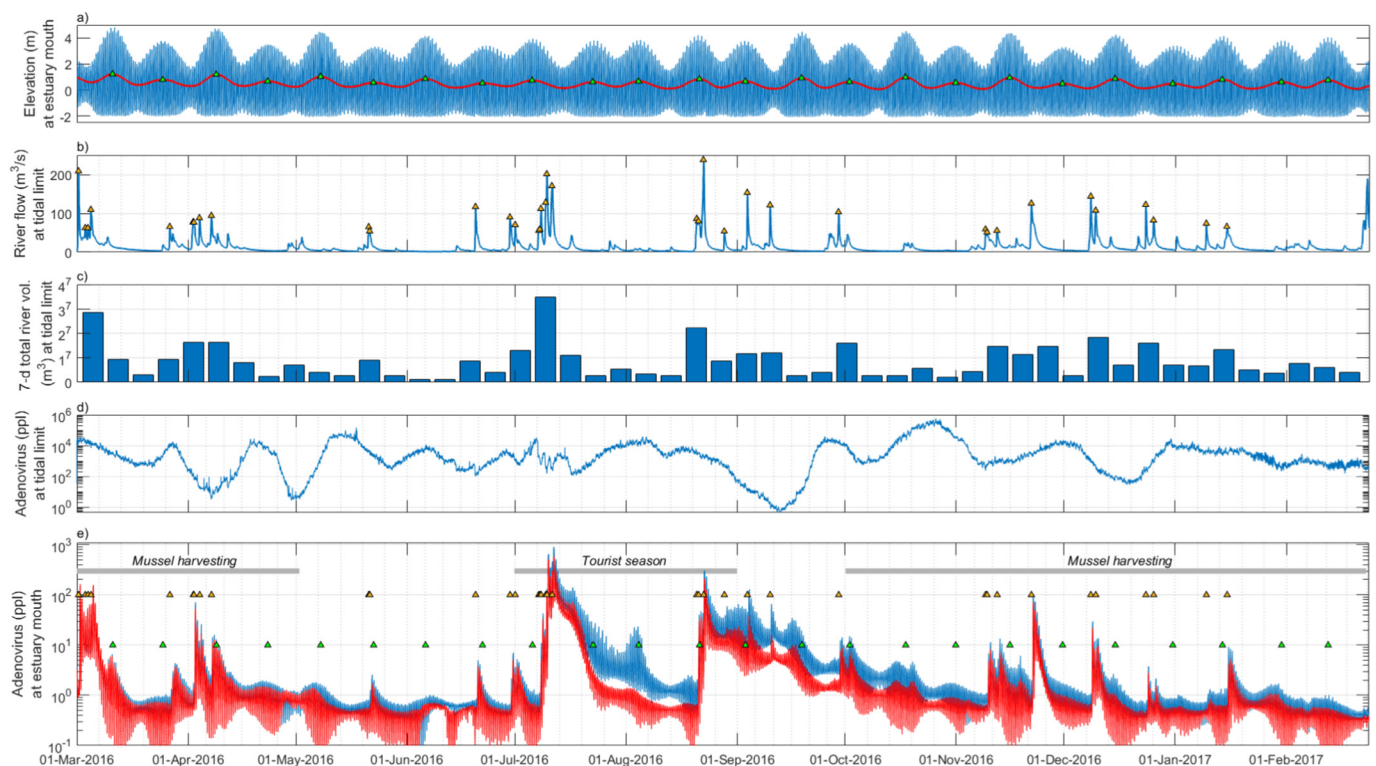

Fig. 2. (a) Simulated surface elevation at the estuary mouth (blue curve; in m relative to MSL) and the tidally-averaged value (red curve); (b) measured river flow ($\text{m}^3\,\text{s}^{-1}$) at the tidal limit; (c) corresponding 7-day river volume (m^3); (d) inputted adenovirus concentration (viral particles per litre; ppl) at the tidal limit; and (e) simulated adenovirus concentration (ppl) at the estuary mouth (the blue curve denotes conservative tracers and the red curve denotes tracers with a decay rate ($T_{90} = 1$ d). Times of peak spring tide and peak river flows above $50\,\text{m}^3\,\text{s}^{-1}$ (green and yellow markers, respectively) are labelled in (a), (b), and (e) for visualisation of key periods. (For interpretation of the references to color in this figure legend, the reader is referred to the web version of this article.)

river, but also influenced by the weather pattern during the preceding few weeks (which was generally wet up to 20 Nov but dry for the few weeks afterwards).

Water fluxes through the estuary mouth were controlled by tidal advection with flow directed landwards during the flooding phase and seaward during the ebbing phase. Consequently, viruses were only exported to the sea during the ebbing tide, although some of the viruses re-entered the estuary during the subsequent flooding tide. Spring tides generated stronger tidal fluxes than neap tides, with larger concentrations of the virus being transported seaward during the ebbing spring tide than the ebbing neap tide. Indeed, some of the simulated peaks in virus concentrations at the mouth occurred during spring tides without large river events (e.g., 05 Aug; 16 Sep; 17 Oct). Conversely, spring flood tides reduced the simulated concentrations at the mouth compared with simulated concentrations during neap flood tides. The tidal influence can therefore be thought of as a background modulator of virus dispersal.

Any seasonal variability in either the river flow regime or the virus concentrations was not apparent from the available data. Consequently, we simulated no seasonality in the viral distributions. Of note, however, was that very large virus concentrations (e.g., 10^6 ppl inputted into the upper estuary on 24 Oct) did not necessarily lead to large virus export from the estuary mouth. Simulated virus transport with a decay function included ($T_{90} = 1$ day) followed the same pattern as described above, albeit with virus concentrations at the estuary mouth decreasing in accordance with Eq. (1). The two virus simulations (with and without a decay function) can be viewed as upper and lower bounds of the likely virus dispersal.

To characterise the spatial variability in simulated dispersal of the virus over the year, we calculated the spatial probability of exceedance for a threshold concentration of 1 ppl (Fig. 3). A significant result was that, for the majority of the year, the virus did not disperse far from the estuary. The 15-day period with the least accumulated virus concentration (starting 13 June) simulated the entire virus concentration to be retained within the estuary (Fig. 3a). When a decay function ($T_{90} = 1$ day) was included, the accumulated virus concentrations were less than with no decay function and the majority of the virus remained ~3 km upstream of the mouth (Fig. 3b).

Only during a few occasions throughout the year were significant simulated virus concentrations exported offshore from the estuary. For the 15-day period with the most accumulated concentration (starting 26 September), regions with a probability of exceedance > 10% tended to be near-shore (i.e., < 5 km away from the coast and up to 30 km along-shore from the estuary mouth). Regions with a probability of exceedance > 50% were generally < 3 km away from the coast (Fig. 3c), which is where shellfishery Sites S1–S7 and beach sites B1–B4 are located. The simulated spatial dispersal of the virus was markedly reduced when a decay function was included, especially in terms of the long-shore dispersal (Fig. 3d).

The total number of days that the simulated virus concentration exceeded 1 ppl was generally > 200 d within the estuary, 100–200 d within ~3 km of the estuary mouth (where S1–S7 and B1–B3 are located), and < 100 d further offshore (Fig. 3e). Note the contour lines in Figs. 3e–h depict where the total number of days exceeds two weeks (14 d). When a decay function was included, the number of days was reduced by 10–30 d offshore, 30–50 d near the mouth/shellfisheries/beaches, and 50–80 d within the estuary (Fig. 3f).

Away from the coast, the maximum continuous duration where the simulated virus concentration exceeded 1 ppl was less than two weeks, although up to 50 d near the mouth where the shellfishery and beach sites are located (Fig. 3g). When a decay function was included, the longest duration of days where the concentration exceeded 1 ppl was reduced by 10–20 d (Fig. 3h).

For the commercial shellfisheries and beach sites, we calculated the probability of exceedance of the simulated virus concentration for different thresholds under the simulated virus inputs (Fig. 4). At the sites

close to the estuary mouth (i.e., within 1 km; shellfishery S1–S7 and beaches B1 and B2), the probability of exceedance of 50 ppl ranged between 1.5% and 3% (for the conservative virus) and between 0.5% and 1.8% (for the virus with a decay function; $T_{90} = 1$ d). The probability of exceedance of 100 ppl ranged between 0.3% and 1% (for conservative virus) and between 0.1% and 0.7% (for the virus with decay). When a viral decay function was included the virus at beaches B1 and B2 only reached 75 ppl (with a probability of exceedance of 0.1%). For beaches further away from the mouth, the conservative virus at B3, and B4 reached 10 and 5 ppl with probabilities of exceedance of 5% and 0.1%, respectively. When decay was included, the virus at these sites reached 5 and 3 ppl with probabilities of exceedance of 5% and 0.1%, respectively.

3.2. Run 2: virus dilution during high river flow events

To test the influence of dilution of the virus concentration by river flow, for Run 2.1 we repeated 30 days of the above simulation (01–30 July 2016) with maximum dilution of the virus. This period was chosen as it coincides with maximum river flows. During the first week of July, river flows were small and there were negligible differences between undiluted and diluted virus concentrations at the estuary mouth (Fig. 5). However, the high flow events the following week combined with a virus concentration that was substantially diluted (to 5–10% of the undiluted concentration) caused virus concentrations at the mouth to be reduced (also to 5–10% of the undiluted concentration). Although the virus concentrations at the estuary mouth were still greater than during low flow events, despite the dilution effect. This is because the virus dispersion is primarily controlled by advection due to the river flow. In the weeks following the high flow event, despite the diluted inflowing virus being of similar concentration to the baseline simulation (in fact, sometimes more concentrated than the baseline simulation after 16 July), the virus concentration at the mouth remained much lower (5–10%) than the baseline virus concentration. This general pattern was also predicted for the analogous simulations with virus decay, albeit with reduced virus concentrations throughout. From this, we conclude that virus concentrations during high river flows are an important control on estuarine virus dispersal for several days following peak river flow.

3.3. Run 3: influence of river flow on viral dispersal

Our annual simulation (Run 1.1) indicated that virus dispersal in the Conwy is controlled by river flow, river viral concentration, and tidal state. To test the relative importance of each control, we conducted a set of hypothetical simulations (see Table 1).

Initially, we wanted to test whether storm clustering had more than an additive effect on viral dispersal out of the estuary. We compared the simulated virus concentrations at the estuary mouth from a single flash river event (Run 3.1) to two back-to-back events with similar peak flows and double the total freshwater volume flux (Run 3.2), as shown in Fig. 6. During the second event on day 2, the virus concentration at the mouth more than doubled (~300%) but increased by ~150% after day 5 (Fig. 6b and c).

Next, we compared the single flash event (Run 3.1) to a cluster of two or three flash events which had lower peak magnitudes than Run 3.1 but the same total freshwater volume flux (Runs 3.3 and 3.4, respectively), as shown in Fig. 6d and e. Our result was predominantly a reduction in virus concentration at the estuary mouth for the cluster events. This is because the peak flow seaward was reduced for the cluster events, compared with the single event; hence, the seaward dispersion distance of the virus was reduced causing a reduced concentration at the mouth (i.e., the virus was concentrated in the upper estuary for the cluster scenarios). Comparing Run 3.1 with Run 3.3, the peak river flow magnitude was halved for Run 3.3 during the first event on day 1, which reduced the virus concentration at the mouth
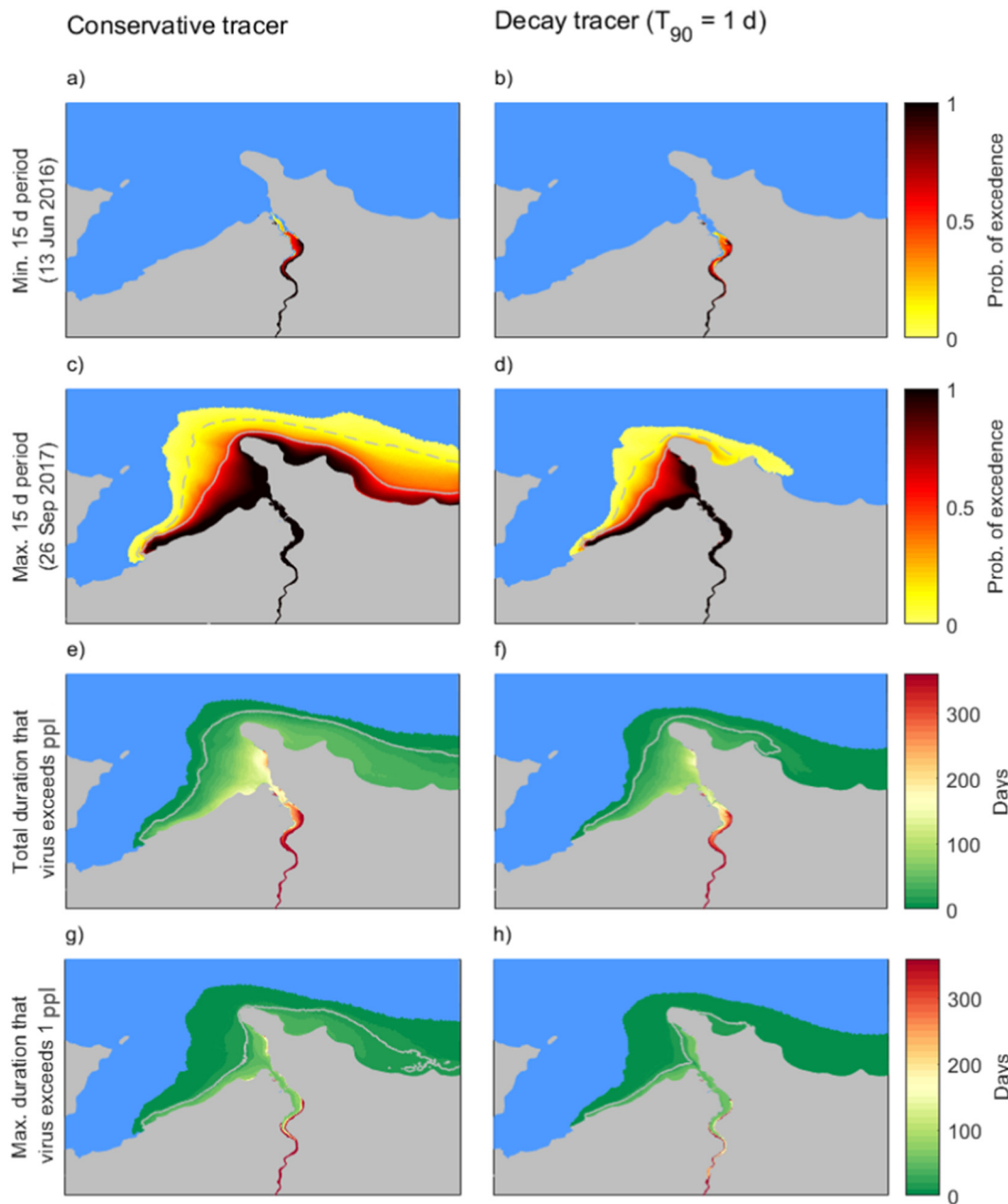
Fig. 3. (a–d): Simulated spatial probability of exceedance of 1 virus particle per litre (ppl) of adenovirus concentration; (a–b) show the 15-day period with minimum virus concentration and (c–d) show the maximum. Contours (in c–d) depict 10% (dashed) and 50% (solid) probabilities of exceeding a virus concentration of 1 ppl. The total number of days where the virus concentration exceeds 1 ppl during 1 year is shown in (e–f), and the maximum continuous duration where concentration exceed 1 ppl is shown in (g–h). Contours (in e–h) depict two weeks (14 d). The left panels show results for conservative tracers and the right panels for tracers with a decay rate (T_{90} = 1 d). All results are based on the year starting 01 March 2016 (Run 1.1).

by > 95%. But the second event for Run 3.3 on day 2 caused the virus concentration at the mouth to be 30% higher than Run 3.1 for a few hours (when there was no peak discharge on day 2). Thereafter, the concentration was generally reduced from Run 3.1 by ~60%. Run 3.4 had three back-to-back events (each with one third of the peak river flow magnitude to Run 3.1), which caused the virus concentration at the mouth to be reduced from Run 3.1 by ~70% (i.e. ~10% lower virus concentrations than for Run 3.3), as explained above. Again, for a short period at the time of the third event on day 3, concentrations at the mouth increased from the other scenarios by a few percent, since those events had no peak discharge on day 3.

Rainfall intensity is also an important control on viral dispersal. When we compared the single flash river event (Run 3.1) with a single slow river event with the same freshwater volume flux but spread over

a day rather than 12 h (Run 3.5), the virus concentration at the mouth was reduced for the slow event, by ~50% during the first two days and by 10–30% thereafter (Fig. 6f and g). In effect, higher virus concentrations remained in the estuary during the slow (non-flash) river event.

The co-occurrence of (or lag time between) peak river flow at the tidal limit in the upper estuary and high tide at the estuary mouth has been shown in Fig. 7 to influence virus concentrations through the estuary mouth. Initially, we simulated peak river flow, from a flash event shown in Fig. 7a, to occur at the same time as high water springs at the estuary mouth, as shown in Fig. 7b (Run 4.1). We compared this simulation to two simulations where the tide lagged peak river flow by 3 h (Run 4.2) and 6 h (Run 4.3), as shown in Fig. 7b. Co-occurrence of peak river flow and high water (Run 4.1) led to peak virus
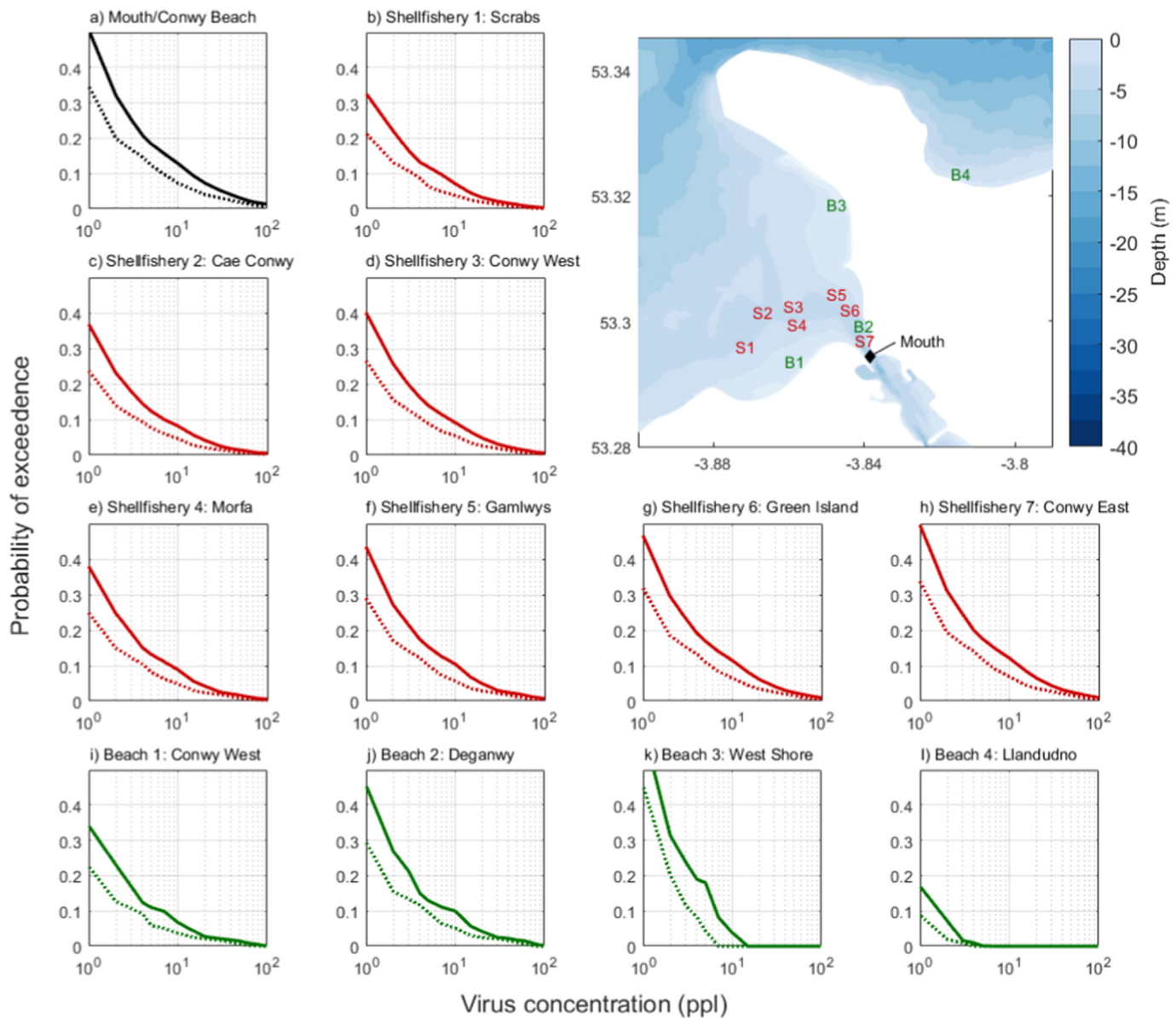
Fig. 4. Probability of exceedance of adenovirus concentrations at (a) the estuary mouth, (b–h) over the shellfishery beds (S1–S7 on inset map), and (i–l) over key coastal tourist beaches (B1–B4 on inset map). Conservative tracers (no viral die-off; solid curves) and tracers with a decay rate (with viral die off; $T_{90} = 1$ d) (dashed curves) are shown. Results are based on the year starting 01 March 2016 (Run 1.1).

concentrations at the mouth of 35 ppl (Fig. 7c). This value doubled with a 3-h lag (Run 4.2) and halved with a 6-h lag. Thereafter (days 2–15), virus concentrations through the estuary mouth were on-average 30% greater with the 3-h lag and 60% greater with the 6-h lag, even though peak virus concentrations were reduced for Run 4.3.

3.4. Run 4: influence of the tide on viral dispersal

We also investigated the influence of the phase of the lunar tidal cycle (i.e., the fortnightly spring-neap cycle). During co-occurrence of peak river flows and high water neaps (Run 4.4), the virus concentration at the mouth was on average 20% higher than co-occurrence of peak river flows and high water springs (Run 4.1), as shown in Fig. 7b and d.

3.5. Run 5: potential worst case event for viral contamination

Finally, we simulated what appeared to be a near 'worst case' event,

in terms of maximal offshore viral dispersal. We simulated the co-occurrence of very large spring tides (tidal range of 6 m) with a cluster of very high river flow events (comprising six events during six days with two peak flows in excess of $400 \, \mathrm{m^3 \, s^{-1}}$) and consistent input virus concentrations of 1×10^5 ppl in the river, with viral decay according to Eq. (1) ($T_{90} = 1$ day). These events correspond to observations in the Conwy river and estuary but recorded at different times, so our simulation (Run 5.1) is hypothetical in the sense that these events could have feasibly coincided. Our results are shown in Fig. 8.

Virus concentrations at the mouth reached 5×10^4 ppl, which was two orders of magnitude higher than during our annual simulation (Run 1.1). The virus concentration remained above 2×10^3 ppl for the remainder of the simulation. Outside the estuary, the virus concentration did not disperse further west than simulated during our annual baseline scenario (e.g., compare Fig. 3d from Run 1.1 with Fig. 8d from Run 5.1). However, there was markedly more eastwards dispersal. We can therefore assume that a virus outbreak in the Conwy catchment under most environmental conditions would remain close to the estuary
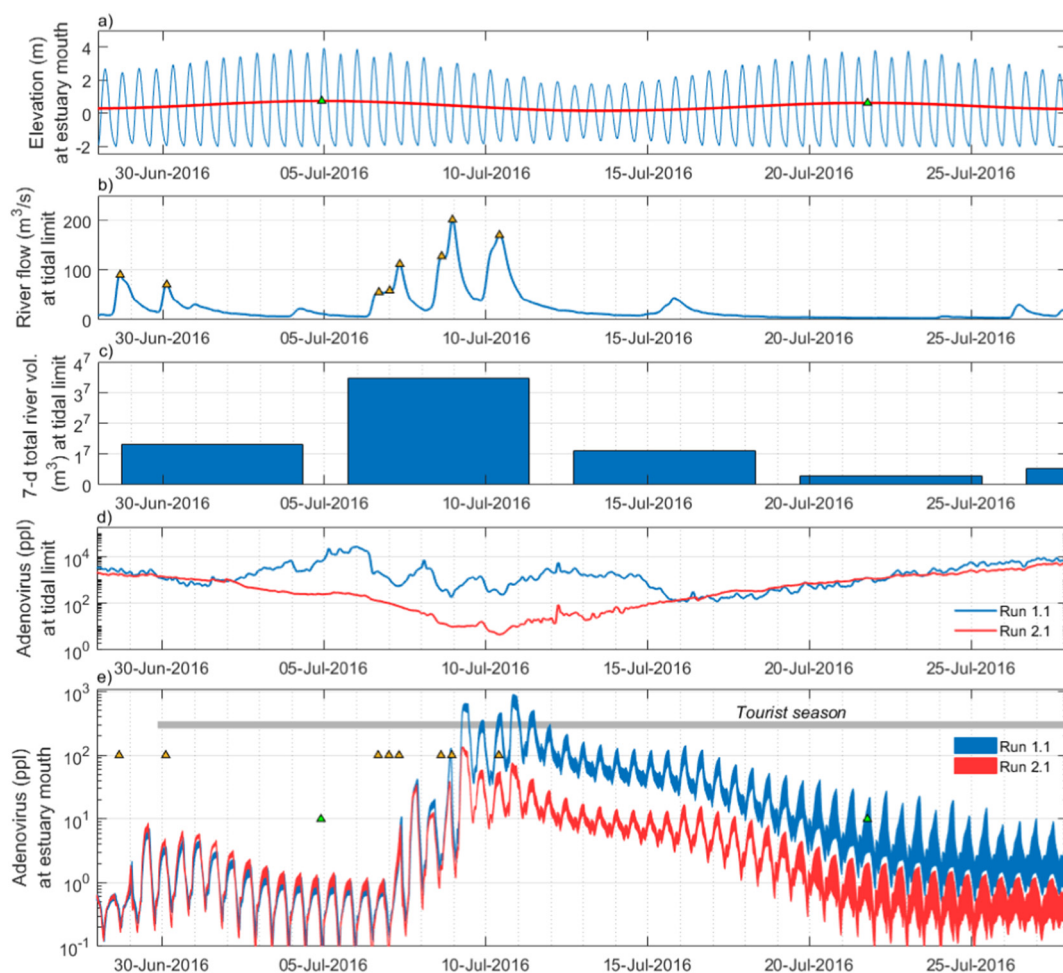
Fig. 5. Run 1.1 vs Run 2.1 (July 2016): (a) Simulated surface elevation at the estuary mouth (blue curve; in m relative to MSL) and the tidally-averaged value (red curve); (b) measured river flow (m^3 s^{-1}) at the tidal limit; (c) corresponding 7-day river volume (m^3); (d) inputted adenovirus concentration (viral particles per litre; ppl) at the tidal limit; and (e) simulated adenovirus concentration (ppl) at the estuary mouth. The upper and lower bounds of each filled curve denote a conservative tracer (no viral die-off) and a tracer with a viral decay rate (T$_{90}$ = 1 d), respectively. Times of peak spring tide and peak river flows above 50 m^3 s^{-1} (green and yellow markers, respectively) are labelled in (a), (b), and (e) for visualisation of key periods. (For interpretation of the references to color in this figure legend, the reader is referred to the web version of this article.)

mouth in a pattern shown in Fig. 8d and e.

4. Discussion

4.1. Role of modelling in viral risk assessment

The quantification of riverine fluxes to the coastal environment is essential for the management of coastal water quality. The assessment of these fluxes, however, is complicated due to the various advection and mixing processes occurring in estuaries (Regnier et al., 1998). Over several tidal cycles (of the order of weeks) the salinity at any point along an estuary is often assumed to be constant implying that the freshwater flow, which acts to freshen the estuary, is balanced by diffusive mechanisms that carry salt landwards (Lewis, 1997). This principle of saline intrusion/estuarine recovery acts to promote the retention of fluvial-sourced viruses within estuaries. It should be noted, however, that in many systems a position of steady-state salt balance/virus retention is rarely achieved due to several factors including regular high fluvial discharge/viral loading events (Regnier et al., 1998; Robins et al., 2018).

We showed for a small and well-mixed estuary that short duration, high intensity fluvial events were the primary control on estuary-ocean viral exchange, although the dispersion mechanisms vary markedly in space and time due to interactions with tidal regime and virus

concentration. We showed that the timing of peak flow relative to the daily and lunar tidal cycles was a secondary control on viral dispersion (i.e., greater estuary-ocean exchange during springs than neaps, and only during ebb tide). This result is in agreement with a model study by Bilgili et al. (2005) on the Great Bay Estuary, US, which is similar in spatial scale to the Conwy – although they noted that complex estuary morphology can complicate the tidal modulation of dispersion. Additional tidal modulations, such as diurnal tidal inequalities (where one tide per day is larger than the other) or monthly tidal modulation (where consecutive lunar tidal cycles are unequal) have also been shown to significantly affect estuary-ocean viral exchange in previous studies (e.g., Regnier et al., 1998).

Based on our results for a small well-mixed estuary, management strategies tasked with future-proofing coastal water quality will require models that incorporate climate projections that resolve high intensity rainfall in combination with tidal and sea level climates. At present, this level of detail is often missing and models rarely capture the magnitude and timing of flash flood events with the temporal scale required to correctly simulate the hydrodynamics and water quality (Lemagie and Lerczak, 2015; Oliver et al., 2016). For similar typologies to the Conwy estuary, increased confidence in future predictions of estuarine mixing and water quality requires rainfall estimates to be downscaled to hourly resolution. This requires the next generation of climate models (e.g. producing convection-permitting rainfall projections) that can improve
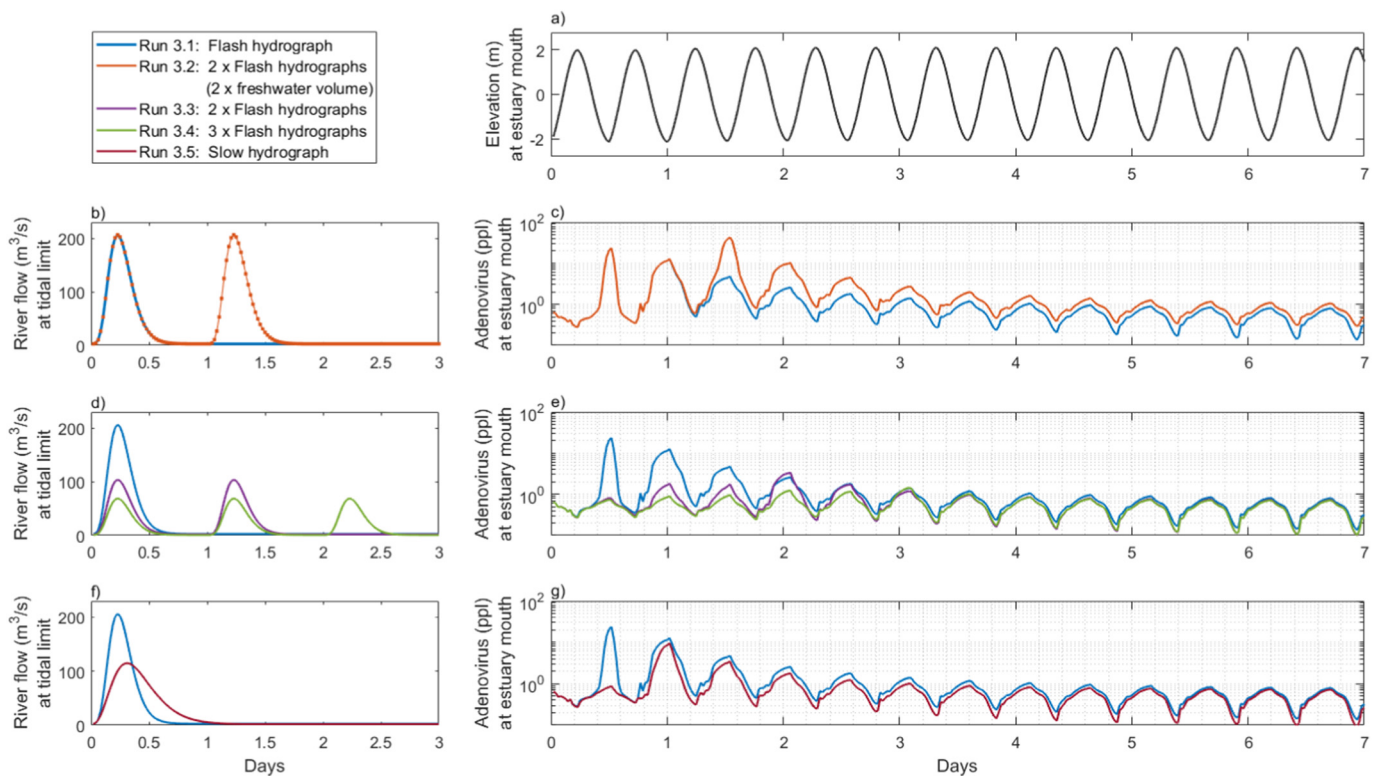
Fig. 6. Run 3: Simulations with consistent tidal forcing (M_2 tidal amplitude = 2 m, as shown in (a)) and constant input virus concentration (at 100 ppl but with decay according to Eq. (1)). We compared virus concentrations at the estuary mouth from a single flash hydrograph versus two consecutive flash hydrographs (b and c); from a single flash hydrograph versus two and three consecutive flash hydrographs with the total freshwater volume constant (d and e); and from a single flash hydrograph versus a single slow hydrographs with the total freshwater volume constant (f and g). Only output during days 1–7 are shown for clearer visualisation.

their relevance to hydrological impact analyses (e.g., Cloke et al., 2013; Charlton and Arnell, 2014; Smith et al., 2014a, 2014b). Then, for example, we can explore the impact of the UK's future projected "drier summers and wetter winters" signal and consequent changes in storm types (e.g., Fowler and Kilsby, 2007; Chan et al., 2013; Kendon et al., 2014), in conjunction with changes in land use and wastewater management.

4.2. Limitations and future research

The movement of viruses through rivers and estuaries can be strongly influenced by absorption to sediment particles or flocs (e.g. which form at the estuarine turbidity maximum; Davies et al., 1995; Anderson et al., 2005). This attachment allows viruses to become protected from harmful UV radiation (Templeton et al., 2005), thereby enhancing their persistence, but also alters their transport via deposition and resuspension in sediments (Drummond et al., 2014). These resuspension events may be a delayed source of pathogens reaching coastal waters (Yamahara et al., 2007) and may also facilitate bioaccumulation in filter feeding shellfish (Rosa et al., 2015). In addition, the interaction of the lateral shear of the longitudinal currents with the axial salinity gradients causes secondary flows that can promote estuary retention of viruses (e.g. Scott, 1994; Turrell et al., 1996). These processes are not considered in our modelling and should be investigated in future studies. Further, we did not include the effects of waves on virus dispersal, although wave effects are thought to be minimal inside the estuary due to the narrow mouth. Outside the estuary, wave heights are usually relatively small (< 3 m) because the coast is sheltered from the predominant southwesterly winds and large Atlantic fetch (Hashemi et al., 2015; Lewis et al., 2017). The largest waves tend to occur following less frequent northwesterly winds. Under such conditions, waves are expected to promote easterly residual transport and hence

easterly dispersal of viruses. For other estuaries, wave-induced flows could be a more important control on virus dispersal and should be taken into account. However, for the purpose of studying the fate of viruses in the Conwy estuary under a range of tidal and hydrological conditions, our described scenario parameterisations are considered adequate.

Another potential limitation of current models is that that they often lack accurate viral discharge data for wastewater treatment plants. This is especially the case for combined sewer overflow events when the wastewater plant either fails or becomes overloaded, releasing raw sewage into the river system (Zhang et al., 2018). In these scenarios, the viral concentrations typically remain similar to the treated effluent (Farkas et al., 2018), however, the viral particles may be less damaged and therefore pose an increased human infection risk. The rate of viral inactivation during passage through the sewage plant and during transport in the river network and in the coastal zone also represents a major knowledge gap. To better evaluate the risk of human infection from contact with contaminated waters it is important to know if the viruses present in the water are infective and how many viral particles need to be ingested to induce disease symptoms. Deactivation of the virus through damage of the viral capsid of nucleic acid material can occur both due to biotic (enzyme degradation) and abiotic processes (e.g. UV irradiation), however, the relative importance of these pathways remains highly dependent on the prevailing weather conditions (e.g. sunlight, temperature) and the degree of chemical and physical protection (Suttle and Feng, 1992; Hijnen et al., 2006; Hassard et al., 2016). While some data exists to enable parameterisation of this (e.g. Bertrand et al., 2012), it remains sparse, especially for viral behaviour in the riverine-estuarine transition zone when flocculation occurs (Hassard et al., 2016). Viral decay is dependent on virus type (DNA vs. RNA viruses), species (e.g. Adenovirus vs. Norovirus) and genotype (e.g. Norovirus GI vs. GII) and consequently the choice of a decay
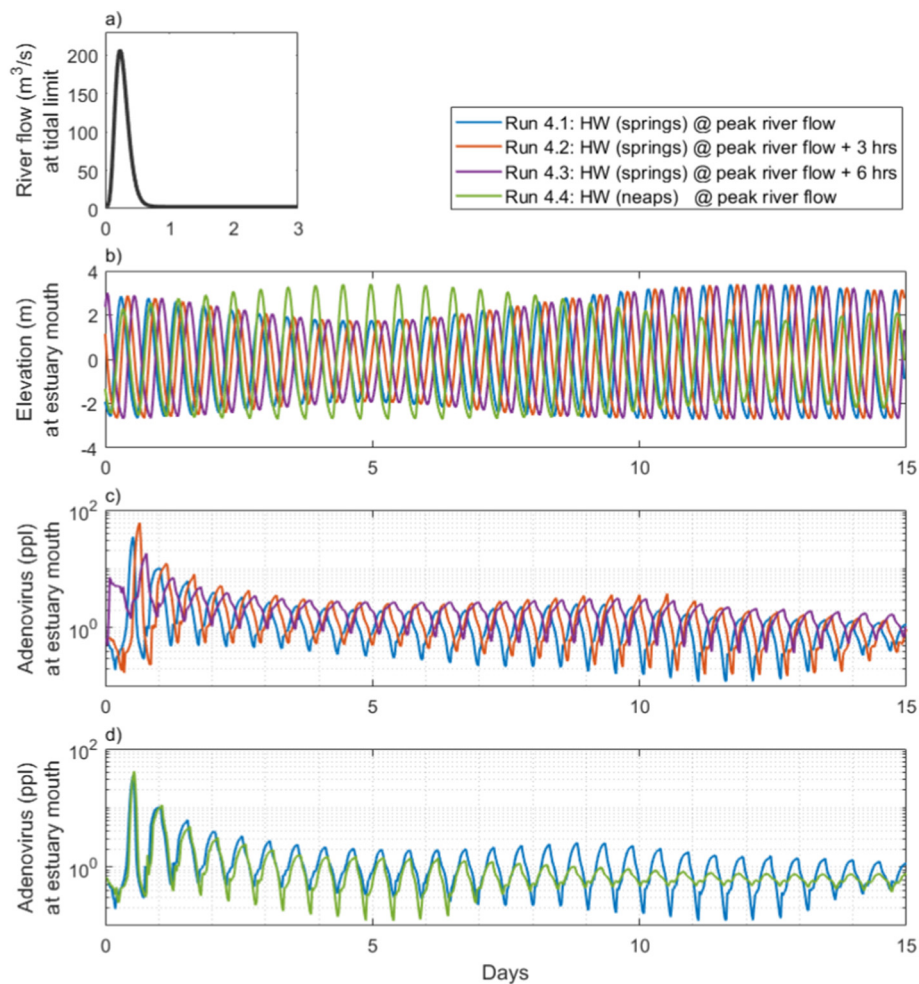
Fig. 7. Run 4: Simulations where we kept river flow forcing consistent (a single flash hydrograph, as shown in (a)) and virus concentration constant (at 100 ppl). We compared elevations and virus concentrations at the estuary mouth when high spring tide occurred at peak river flow versus a high water lag of 3 h and 6 h (b and c); and when high spring tide occurred at peak river flow verses when high neap tide occurred at peak river flow (b and d).

constant (i.e. T_{90} value) can vary greatly both for fresh and marine waters (Meng and Gerba, 1996; Nuanualsuwan et al., 2002). Due to this uncertainty, from a risk assessment perspective it may be best to run scenarios with a zero die-off value (i.e. simply dilute and disperse) and with a relatively rapid die-off (i.e. as used here) to allow prediction of the best and worst case scenarios.

Lastly, the factors affecting the rate of viral capture by shellfish is also highly uncertain and more work is required to parameterise this element of the model.

4.3. Risk assessment and active management

As highlighted above, there are still deficiencies in our understanding of how human pathogenic viruses behave in the wastewater-river-estuary-coastal continuum. While models such as those presented here are useful for examining the importance of specific factors in regulating viral behaviour, our view is that these uncertainties are limiting their potential to be used for the active (i.e. real-time) management of viral pollution in shellfisheries, recreational waters and beaches. The failure to capture the complexity of viral behaviour is exemplified in a previous attempt to undertake quantitative microbial risk assessments (QMRA) for poliovirus release into coastal waters (Duizer et al., 2016). In this study, the model greatly overestimated the risk of human infection. To maintain confidence in QMRA, it is essential that the models are accurate and validated. In this way, false-positives can be avoided, particularly as decisions made on these may have

severe negative economic and cultural consequences (e.g. unnecessary closure of shellfisheries and tourist beaches). It should also be noted that QMRA procedures developed for faecal bacteria are also unsuitable for viruses due to major differences in their behaviour (Winterbourn et al., 2016; Hassard et al., 2017; Leight et al., 2018; Zimmer-Faust et al., 2018).

5. Conclusions

Small, well-mixed estuaries outnumber larger estuaries within many countries. However, models of these systems require time-dependent forcing (e.g. resolving individual fluvial events and tidal cycles) to understand the physical processes leading to episodes of poor water quality. For our case study of the Conwy, we highlight the importance of storm river flow as a major control delivering potentially harmful virus loads to the coast. Episodes of high virus concentrations in the river did not necessarily lead to high virus concentrations offshore during periods of low river flow (i.e., $Q < Q10 = 50\,m^3\,s^{-1}$), as the majority of simulated viruses were retained within the estuary. However, during storms (i.e., $Q > Q10$), we simulated substantial estuary-ocean exchange of viruses (between 5 and 1000 ppl), despite the virus dilution effect in the river. Viruses were exported from the estuary on the ebb tide, most of which re-entered on the following flood and continued in this back-and-forth manner in the vicinity of shellfisheries and beaches. A single high flow event flushed more virus load out to sea than a cluster of smaller events, or an event of lower magnitude and
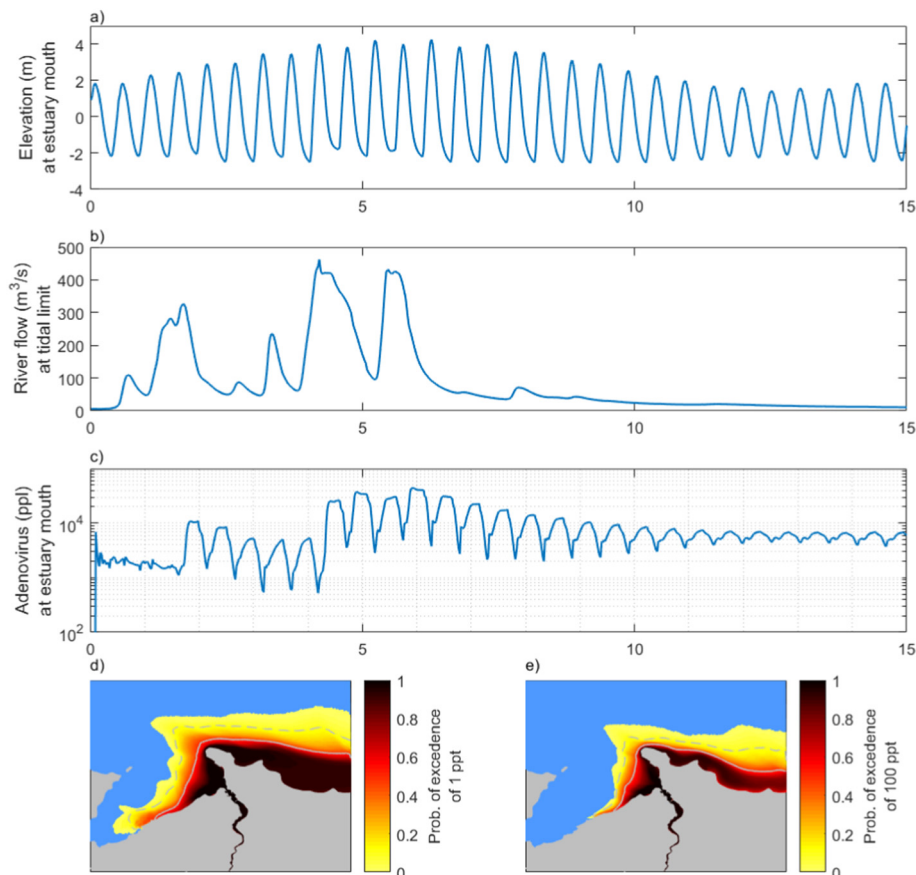
Fig. 8. Run 5: A simulation of a potential combination extreme event. We simulated the co-occurrence of very large spring tides (a) with an observed cluster of very high river flow events (b) and consistent maximum observed virus concentrations in the river (1×10^5 ppl with a virus decay where $T_{90} = 1$ day). Concentrations at the estuary mouth are shown in (c). Spatial maps of probability of exceedance of 1 ppl and 100 ppl are shown in panels (d) and (e), respectively. Contours (in d–e) depict a 10% (dashed) or 50% (solid) probability of exceeding a virus concentration of 1 ppl.

longer duration, amounting to the same virus flux. Risk of poor water quality near shellfisheries and beaches is therefore heightened following a single river event with peak flows greater than ~Q10, and risk is increased further following clusters of such events. Short duration, high intensity river flows heighten the coastal water quality risk. Coincident peak flows in the river and high spring tide at the mouth, rather than neap tide, caused the highest simulated virus concentrations to be transported out of the estuary (actually phased-occurrence of peak flows and tides, with the phase lag roughly dependent on the length of the estuary). In this case, viruses can remain in the coastal zone for up to 50 d, depending on die-off rates. Variability within the inflowing virus concentration (e.g., due to a virus outbreak) was less of a control than river flow on the overall export of viruses.

Acknowledgements

References

Adriaenssens, E.M., Farkas, K., Harrison, C., Jones, D.L., Allison, H.E., McCarthy, A.J., 2018. Viromic analysis of wastewater input to a river catchment reveals a diverse assemblage of RNA Viruses. mSystems 3, e00025-18.

Anderson, K.L., Whitlock, J.E., Harwood, V.J., 2005. Persistence and differential survival of fecal indicator bacteria in subtropical waters and sediments. Appl. Environ. Microbiol. 71, 3041–3048.

Bertrand, I., Schijven, J.F., Sánchez, G., Wyn-Jones, P., Ottoson, J., Morin, T., Muscillo, M., Verani, M., et al., 2012. The impact of temperature on the inactivation of enteric viruses in food and water: a review. J. Appl. Microbiol. 112, 1059–1074.

Bilgili, A., Proehl, J.A., Lynch, D.R., Smith, K.W., Swift, M.R., 2005. Estuary/ocean exchange and tidal mixing in a Gulf of Maine Estuary: a Lagrangian modeling study. Estuar. Coast. Shelf Sci. 65, 607–624.

Bofill-Mas, S., Albinana-Gimenez, N., Clemente-Casares, P., Hundesa, A., Rodriguez-Manzano, J., Allard, A., Calvo, M., Girones, R., 2006. Quantification and stability of human adenoviruses and polyomavirus JCPyV in wastewater matrices. Appl. Environ. Microbiol. 72, 7894–7896.

Burchard, H., Bolding, K., Feistel, R., Gräwe, U., Klingbeil, K., MacCready, P., Mohrholz, V., Umlauf, L., van der Lee, E.M., 2018. The Knudsen theorem and the Total Exchange Flow analysis framework applied to the Baltic Sea. Prog. Oceanogr. 165, 268–286.

Chan, S.C., Kendon, E.J., Fowler, H.J., Blenkinsop, S., Ferro, C.A., Stephenson, D.B., 2013. Does increasing the spatial resolution of a regional climate model improve the simulated daily precipitation? Clim. Dyn. 41, 1475–1495.

Charles, K.J., Shore, J., Sellwood, J., Laverick, M., Hart, A., Pedley, S., 2009. Assessment of the stability of human viruses and coliphage in groundwater by PCR and infectivity methods. J. Appl. Microbiol. 106, 1827–1837.

Charlton, M.B., Arnell, N.W., 2014. Assessing the impacts of climate change on river flows in England using the UKCP09 climate change projections. J. Hydrol. 519, 1723–1738.

Cloke, H.L., Wetterhall, F., He, Y., Freer, J.E., Pappenberger, F., 2013. Modelling climate impact on floods with ensemble climate projections. Q. J. R. Meteorol. Soc. 139, 282–297.

Davidson, N.C., Laffoley, D.D.A., Doody, J.P., Way, L.S., Gordon, J., Key, R.E., Drake, C.M., Pienkowski, M.W., Mitchell, R., Duff, K.L., 1991. Nature Conservation and Estuaries in Great Britain. Nature Conservancy Council, Peterborough, UK.

Davies, C.M., Long, J.A., Donald, M., Ashbolt, N.J., 1995. Survival of fecal microorganisms in marine and freshwater sediments. Appl. Environ. Microbiol. 61, 1888–1896.

Drummond, J.D., Davies-Colley, R.J., Stott, R., Sukias, J.P., Nagels, J.W., Sharp, A., Packman, A.I., 2014. Retention and remobilization dynamics of fine particles and microorganisms in pastoral streams. Water Res. 66, 459–472.

Duizer, E., Rutjes, S., Husman, A.M.D., Schijven, J., 2016. Risk assessment, risk management and risk-based monitoring following a reported accidental release of

poliovirus in Belgium, September to November 2014. Eurosurveillance 21, 16–26.

EDINA, 2008. In: EDINA (Ed.), Marine Digimap Service, Hydrospatial Bathymetry, Scale 1: 45,000, Tiles: NW25000040-NW25000080, NW25200040-NW25200080, NW25400040 NW25400080. SeaZone Solutions Ltd., UK Updated April 2008.

Egbert, G.D., Bennett, A.F., Foreman, M.G., 1994. TOPEX/POSEIDON tides estimated using a global inverse model. J. Geophys. Res. 99, 24821–24852.

Eischeid, A.C., Thurston, J.A., Linden, K.G., 2011. UV disinfection of adenovirus: present state of the research and future directions. Crit. Rev. Environ. Sci. Technol. 41, 1375–1396.

Emmett, B.A., Cooper, D., Smart, S., Jackson, B., Thomas, A., Cosby, B., Evans, C., Glanville, H., McDonald, J.E., Malham, S.K., Marshall, M., Jarvis, S., Rajko-Nenow, P., Webb, G.P., Ward, S., Rowe, E., Jones, L., Vanbergen, A.J., Keith, A., Carter, H., Pereira, M.G., Hughes, S., Lebron, I., Wade, A., Jones, D.L., 2016. Spatial patterns and environmental constraints on ecosystem services at a catchment scale. Sci. Total Environ. 572, 1586–1600.

Enriquez, C.E., Hurst, C.J., Gerba, C.P., 1995. Survival of the enteric adenoviruses 40 and 41 in tap, sea, and waste water. Water Res. 29, 2548–2553.

Farkas, K., Cooper, D.M., McDonald, J.E., Malham, S.K., de Rougemont, A., Jones, D.L., 2018. Seasonal and spatial dynamics of enteric viruses in wastewater and in riverine and estuarine receiving waters. Sci. Total Environ. 634, 1174–1183.

Fowler, H.J., Kilsby, C.G., 2007. Using regional climate model data to simulate historical and future river flows in northwest England. Clim. Chang. 80, 337–367.

Griffin, D.W., Donaldson, K.A., Paul, J.H., Rose, J.B., 2003. Pathogenic human viruses in coastal waters. Clin. Microbiol. Rev. 16, 129–143.

Hashemi, M.R., Neill, S.P., Robins, P.E., Davies, A.G., Lewis, M.J., 2015. Effect of waves on the tidal energy resource at a planned tidal stream array. Renew. Energy 75, 626–639.

Hassard, F., Gwyther, C.L., Farkas, K., Andrews, A., Jones, V., Cox, B., Brett, H., Jones, D.L., McDonald, J.E., Malham, S.K., 2016. Abundance and distribution of enteric bacteria and viruses in coastal and estuarine sediments - a review. Front. Microbiol. 7, 1692.

Hassard, F., Sharp, J.H., Taft, H., LeVay, L., Harris, J.P., McDonald, J.E., Tuson, K., Wilson, J., Jones, D.L., Malham, S.K., 2017. Critical review on the public health impact of norovirus contamination in shellfish and the environment: a UK perspective. Food Environ. Virol. 9, 123–141.

Henry, R., Schang, C., Coutts, S., Kolotelo, P., Prosser, T., Crosbie, N., Grant, T., Cottam, D., O'Brien, P., Deletic, A., McCarthy, D., 2016. Into the deep: evaluation of SourceTracker for assessment of faecal contamination of coastal waters. Water Res. 93, 242–253.

Hervouet, J., 2007. Hydrodynamics of Free Surface Flows. John Wiley & Sons, London, UK.

Hijnen, W.A.M., Beerendonk, E.F., Medema, G.J., 2006. Inactivation credit of UV radiation for viruses, bacteria and protozoan (oo)cysts in water: a review. Water Res. 40, 3–22.

Howlett, E.R., Bowers, D.G., Malarkey, J., Jago, C.F., 2015. Stratification in the presence of an axial convergent front: causes and implications. Estuar. Coast. Shelf Sci. 161, 1–10.

Kendon, E.J., Roberts, N.M., Fowler, H.J., Roberts, M.J., Chan, S.C., Senior, C.A., 2014. Heavier summer downpours with climate change revealed by weather forecast resolution model. Nat. Clim. Chang. 4, 570–576.

Kitajima, M., Iker, B.C., Pepper, I.L., Gerba, C.P., 2014. Relative abundance and treatment reduction of viruses during wastewater treatment processes—identification of potential viral indicators. Sci. Total Environ. 488, 290–296.

Landry, E.F., Vaughn, J.M., Vicale, T.J., Mann, R., 1983. Accumulation of sediment-associated viruses in shellfish. Appl. Environ. Microbiol. 45, 238–247.

Leight, A.K., Crump, B.C., Hood, R.R., 2018. Assessment of fecal indicator bacteria and potential pathogen co-occurrence at a shellfish growing area. Front. Microbiol. 9, 384.

Lemagie, E.P., Lerczak, J.A., 2015. A comparison of bulk estuarine turnover timescales to particle tracking timescales using a model of the Yaquina Bay Estuary. Estuar. Coasts 38, 1797–1814.

Lewis, J., 1997. Dispersion in Estuaries and Coastal Waters. John Wiley & Sons, London.

Lewis, M., Neill, S.P., Robins, P., Hashemi, M.R., Ward, S., 2017. Characteristics of the velocity profile at tidal-stream energy sites. Renew. Energy 114, 258–272.

Linden, K.G., Thurston, J., Schaefer, R., Malley, J.P., 2007. Enhanced UV inactivation of adenoviruses under polychromatic UV lamps. Appl. Environ. Microbiol. 73, 7571–7574.

MacCready, P., Rockwell Geyer, W., Burchard, H., 2018. Estuarine exchange flow is related to mixing through the salinity variance budget. J. Phys. Oceanogr. 48, 1375–1384.

Meng, Q.S., Gerba, C.P., 1996. Comparative inactivation of enteric adenoviruses, poliovirus and coliphages by ultraviolet irradiation. Water Res. 30, 2665–2668.

Nuanualsuwan, S., Mariam, T., Himathongkham, S., Cliver, D.O., 2002. Ultraviolet inactivation of feline calicivirus, human enteric viruses and coliphages. Photochem. Photobiol. 76, 406–410.

Oliveira, J., Cunha, A., Castilho, F., Romalde, J.L., Pereira, M.J., 2011. Microbial contamination and purification of bivalve shellfish: crucial aspects in monitoring and future perspectives – a mini-review. Food Control 22, 805–816.

Oliver, D.M., Porter, K.D., Pachepsky, Y.A., Muirhead, R.W., Reaney, S.M., Coffey, R., Kay, D., Milledge, D.G., Hong, E., Anthony, S.G., Page, T., 2016. Predicting microbial water quality with models: over-arching questions for managing risk in agricultural catchments. Sci. Total Environ. 544, 39–47.

Qiu, Y., Lee, B.E., Neumann, N., Ashbolt, N., Craik, S., Maal-Bared, R., Pang, X.L., 2015. Assessment of human virus removal during municipal wastewater treatment in Edmonton, Canada. J. Appl. Microbiol. 119, 1729–1739.

Rachmadi, A.T., Torrey, J.R., Kitajima, M., 2016. Human polyomavirus: advantages and limitations as a human-specific viral marker in aquatic environments. Water Res. 456–469.

Rames, E., Roiko, A., Stratton, H., Macdonald, J., 2016. Technical aspects of using human adenovirus as a viral water quality indicator. Water Res. 96, 308–326.

Rastogi, A.K., Rodi, W., 1978. Predictions of heat and mass transfer in open channels. J. Hydraul. Div. 104, 397–420.

Regnier, P., Mouchet, A., Wollast, R., Ronday, F., 1998. A discussion of methods for estimating residual fluxes in strong tidal estuaries. Cont. Shelf Res. 18, 1543–1571.

Rigotto, C., Hanley, K., Rochelle, P.A., De Leon, R., Barardi, C.R.M., Yates, M.V., 2011. Survival of adenovirus types 2 and 41 in surface and ground waters measured by a plaque assay. Environ. Sci. Technol. 45, 4145–4150.

Robins, P.E., Lewis, M.J., Simpson, J.H., Howlett, E.R., Malham, S.K., 2014. Future variability of solute transport in a macrotidal estuary. Estuar. Coast. Shelf Sci. 151, 88–99.

Robins, P.E., Skov, M.W., Lewis, M.J., Giménez, L., Davies, A.G., Malham, S.K., Neill, S.P., McDonald, J.E., Whitton, T.A., Jackson, S.E., Jago, C.F., 2016. Impact of climate change on UK estuaries: a review of past trends and potential projections. Estuar. Coast. Shelf Sci. 169, 119–135.

Robins, P.E., Lewis, M.J., Freer, J., Cooper, D.M., Skinner, C.J., Coulthard, T.J., 2018. Improving estuary models by reducing uncertainties associated with river flows. Estuar. Coast. Shelf Sci. 207, 63–73.

Rosa, M., Ward, J.E., Ouvrard, M., Holohan, B.A., Espinosa, E.P., Shumway, S.E., Allam, B., 2015. Examining the physiological plasticity of particle capture by the blue mussel, *Mytilus edulis* (L.): confounding factors and potential artifacts with studies utilizing natural seston. J. Exp. Mar. Biol. Ecol. 473, 207–217.

Scott, C.F., 1994. A numerical study of the interaction of tidal oscillations and non-linearities in an estuary. Estuar. Coast. Shelf Sci. 36, 477–496.

Simpson, J.H., Vennell, R., Souza, A.J., 2001. The salt fluxes in a tidally energetic estuary. Estuar. Coast. Shelf Sci. 52, 131–142.

Smith, A., Bates, P., Freer, J., Wetterhall, F., 2014a. Investigating the application of climate models in flood projection across the UK. Hydrol. Process. 28, 2810–2823.

Smith, A., Freer, J., Bates, P., Sampson, C., 2014b. Comparing ensemble projections of flooding against flood estimation by continuous simulation. J. Hydrol. 511, 205–219.

Suttle, C.A., Feng, C., 1992. Mechanisms and rates of decay of marine viruses in seawater. Appl. Environ. Microbiol. 58, 3721–3729.

Templeton, M.R., Andrews, R.C., Hofmann, R., 2005. Inactivation of particle-associated viral surrogates by ultraviolet light. Water Res. 39, 3487–3500.

Turrell, W.R., Brown, J., Simpson, J.H., 1996. Salt intrusion and secondary flow in a shallow, well-mixed estuary. Estuar. Coast. Shelf Sci. 42, 153–169.

Wait, D.A., Sobsey, M.D., 2001. Comparative survival of enteric viruses and bacteria in Atlantic Ocean seawater. Water Sci. Technol. 43, 139–142.

WHO, 2015. WHO Estimates of the Global Burden of Foodborne Diseases Foodborne Diseases Burden Epidemiology Reference Group 2007–2015. World Health Organisation, Rome.

Winterbourn, J.B., Clements, K., Lowther, J.A., Malham, S.K., McDonald, J.E., Jones, D.L., 2016. Use of *Mytilus edulis* biosentinels to investigate spatial patterns of norovirus and faecal indicator organism contamination around coastal sewage discharges. Water Res. 105, 241–250.

Yamahara, K.M., Layton, B.A., Santoro, A.E., Boehm, A.B., 2007. Beach sands along the California coast are diffuse sources of fecal bacteria to coastal waters. Environ. Sci. Technol. 41, 4515–4521.

Zhang, D., Holland, E.S., Lindholm, G., Ratnaweera, H., 2018. Hydraulic modeling and deep learning based flow forecasting for optimizing inter catchment wastewater transfer. J. Hydrol. 567, 792–802.

Zimmer-Faust, A.G., Brown, C.A., Manderson, A., 2018. Statistical models of fecal coliform levels in Pacific Northwest estuaries for improved shellfish harvest area closure decision making. Mar. Pollut. Bull. 137, 360–369.